

Robust Blur Kernel Estimation for License Plate Images from Fast Moving Vehicles

Qingbo Lu, Wengang Zhou, Lu Fang, and Houqiang Li, *Senior Member, IEEE*

Abstract—As the unique identification of a vehicle, license plate is a key clue to uncover over-speed vehicles or the ones involved in hit-and-run accidents. However, the snapshot of over-speed vehicle captured by surveillance camera is frequently blurred due to fast motion, which is even unrecognizable by human. Those observed plate images are usually in low resolution and suffer severe loss of edge information, which cast great challenge to existing blind deblurring methods. For license plate image blurring caused by fast motion, the blur kernel can be viewed as linear uniform convolution and parametrically modeled with angle and length. In this paper, we propose a novel scheme based on sparse representation to identify the blur kernel. By analysing the sparse representation coefficients of the recovered image, we determine the angle of the kernel based on the observation that the recovered image has the most sparse representation when the kernel angle corresponds to the genuine motion angle. Then, we estimate the length of the motion kernel with Radon transform in Fourier domain. Our scheme can well handle large motion blur even when the license plate is unrecognizable by human. We evaluate our approach on real-world images and compare with several popular state-of-the-art blind image deblurring algorithms. Experimental results demonstrate the superiority of our proposed approach in terms of effectiveness and robustness.

Index Terms—Kernel parameter estimation, license plate deblurring, linear motion blur, sparse representation.

I. INTRODUCTION

License plate is the unique ID of each vehicle and plays a significant role in identifying the trouble-maker vehicle. Nowadays, there are lots of auto over-speed detection and capture systems for traffic violation on the main roads of cities and high-ways. However, the motion of vehicle during the exposure time would cause the blur of snapshot image. Therefore, the exposure time (shutter speed) has significant impact on the amount of blur. For video shooting, the exposure time is largely dependent on the illumination situations. In usual outdoor scene with sunshine, the typical exposure time is about 1/300 second. For a vehicle running at 60 miles per



Fig. 1: One example of fast-moving vehicle image and our final deblurred result.

hour, during the exposure time, the displacement of license plate is about 9 centimeters which is comparable with the size of the license plate (14 × 44 centimeters in China), *i.e.*, the length of kernel is about 45 pixels when the license plate image is with size of 140 × 440 pixels and the angle between camera imaging plane and horizontal plane is about 60 degree. In such a scenario, the blur of license plate cannot be neglected. In an ideal scenario with sound illumination, the blur from shorter exposure time, say, 1/1000 second, can be minor and may not damage the semantic information. However, under poor illumination situations, the camera has to prolong the exposure time to obtain a fully exposed image, which easily incurs the motion blur. Besides, for high-resolution digital cameras, high-speed videography is also susceptible to motion blur [1]. When the vehicle is over-speeded, such blurring effect from fast motion becomes much more severe, resulting in plates far from detectable, recognizable and difficult for retrieval [2]–[5]. In this scenario, the fundamental task of license plate deblurring is to recover the useful semantic clue for identification. For example, for a blurred snapshot of over-speed vehicle, the most important issue is to recognize its license plate after image deblurring.

In the last decades, blind image deblurring/deconvolution (BID) has gained lots of attention from the image processing community. Although some advances have been made, it is still very challenging to address many real-world cases. Mathematically, the model of image blurring can be formulated as:

$$B(x, y) = (k * I)(x, y) + G(x, y) \quad (1)$$

where B , I , and k denote the blurred image, the sharp image we intend to recover, and the blur kernel, respectively; G is the additive noise (usually regarded as white Gaussian noise); and $*$ denotes convolution operator. For BID, the kernel k and sharp image I are both unknown. According to whether the kernel k is spatially-invariant or not, the BID problem can be divided into two categories: uniform BID and non-uniform

Manuscript received January 20, 2015; revised July 23, 2015 and November 7, 2015; accept February 10, 2016. This work was supported in part to Prof. Houqiang Li by 973 Program under Contract 2015CB351803, Natural Science Foundation of China (NSFC) under Contract No. 61390514, and Contract No. 61325009, in part to Dr. Wengang Zhou by NSFC under contract No. 61472378, Anhui Provincial Natural Science Foundation under contract No. 1508085MF109, and the Fundamental Research Funds for the Central Universities, and in part to Dr. Lu Fang by NSFC under Contract No. 61303151 and No. 61331015. The associate editor coordinating the review of this manuscript and approving it for publication was Dr. Damon Chandler.

Q. Lu, W. Zhou, L. Fang and H. Li are with the CAS Key Laboratory of Technology in Geo-spatial Information Processing and Application System, University of Science and Technology of China, Hefei 230027, China. (email: luqingbo@mail.ustc.edu.cn; zhwg@ustc.edu.cn; fanglu@ustc.edu.cn; lihq@ustc.edu.cn; Professor Houqiang Li is the corresponding author).

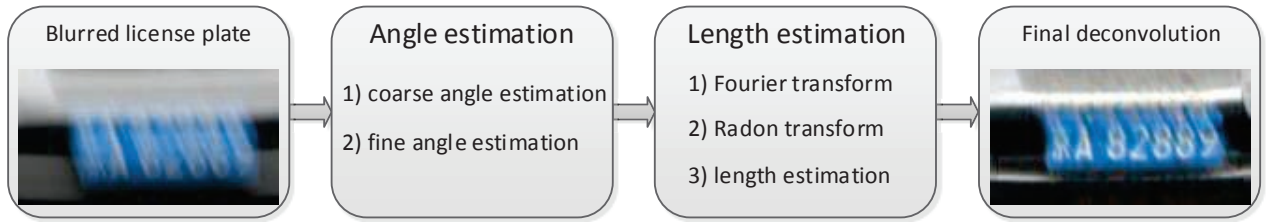


Fig. 2: Flow chart of the proposed method.

BID. For uniform BID, the kernel k is often called point spread function.

In recent years, many effective BID algorithms have been proposed. Due to the ill-posed nature of BID, prior knowledge is usually introduced to avoid falling into the incorrect solutions. Most of them simultaneously estimate kernel from the blurred image and apply a non-blind image deblurring (NBID) algorithm recursively to approach the true solution [6]–[10]. Another alternative is to take a two-step strategy, in which the key point is to estimate an accurate kernel, then NBID algorithm is only applied once to obtain the final restored image [11]–[13].

Compared with the classical BID problems, license plate deblurring has its own distinctive characteristics. Fig. 1 shows one example of images on fast moving vehicle in a real scenario. In this scenario, instead of improving the visual quality, we are more interested in generating a recognizable result. The challenges for license plate deblurring lie in three aspects.

- 1) The surveillance camera is usually designed for capturing a big scene that includes a whole vehicle, therefore, the license plate only occupies a small region of the whole image. This leads to insufficient details for kernel estimation.
- 2) Due to the fast motion, the size of blur kernel is very large. The edge information is degraded severely and is unavailable from blurred images. Therefore, the methods based on large scale edges cannot work robustly and even may fail in some situations [14].
- 3) The content of licence plate image is very simple, most of edges lie in horizontal and vertical directions. Thus, the methods based on isotropy assumption [12] may also not work well for license plate image.

In this paper, we target on this challenging BID problem: blind deblurring of fast moving license plate, which is severely blurred and even unrecognizable by human. Our goal is to recover a sharp license plate with confidence that the restored license plate image can be recognized by human effortlessly. Generally speaking, the blur kernel is dominated by the relative motion between the moving car and static surveillance camera, which can be modeled as a projection transform [15]. However, the kernel can be approximated by linear uniform motion blur kernel. The task of blur kernel estimation can be reduced to the estimation of two parameters in the linear motion kernel: angle (θ) and length (l). Given a linear kernel $k_{\theta,l}$, a corresponding deblurred image $\hat{I}_{\theta,l}$ can be obtained by applying NBID on the blurred image B with $k_{\theta,l}$. Then

the sparse representation coefficients of $\hat{I}_{\theta,l}$ on pre-trained dictionary can be denoted as $A(\theta, l)$, which is a function of θ and l . We observe that $A(\theta, l)$ shows very useful quasi-convex characteristic under a fixed l . By utilizing this interesting characteristic, we can infer the true angle of the blur kernel efficiently. Once the angle is determined, on the direction parallel to the motion, the power spectrum of blurred image is obviously affected by the linear kernel based on which the spectrum is a sinc-like function, and the distance between its two adjacent zero-crossings in frequency domain is determined by the length of kernel. In order to reduce the effect of noise and improve the robustness of length estimation, we utilize the Radon transform in frequency domain. After kernel estimation, we obtain the final deblurring result with a very simple NBID algorithm.

The rest of this paper is organized as follows. In Section II, we review several popular methods about BID and kernel parameter estimation. In Section III, we introduce the useful property of sparse representation coefficients and present our kernel parameter estimation in detail. Deblurring results and comparing experiments with the state-of-the-art blind image deblurring algorithms are provided in Section IV. Finally, we conclude this paper in Section V.

II. RELATED WORK

From the perspective of Bayesian inference, there are two main alternatives for BID: maximum a posteriori (MAP) methods and marginalization methods. On the other hand, for specific kernel, the recovery can be reduced to a parameter estimation problem. In this section, we will review several representative BID schemes in the above three categories.

A. MAP methods

The MAP methods attempt to obtain the latent image by solving the following optimization problem:

$$(\hat{k}, \hat{I}) = \underset{k, I}{\operatorname{argmax}} \{p(k, I|B) \propto p(B|k, I)p(k)p(I)\} \quad (2)$$

where $p(B|k, I)$ is the likelihood item which is usually modeled with a Gaussian distribution; $p(k)$ and $p(I)$ denote the prior knowledge of kernel and latent image, respectively.

As Levin *et al.* [11] pointed out, the solution of naive MAP framework with gradient sparsity prior usually does not necessarily correspond to the kernel and sharp image, but leads to the result favoring the “no blur” solution ($\hat{I} = B$). To avoid obtaining a “no blur” solution, several preprocessing methods have been proposed for the MAP framework. Shan *et al.* [7]

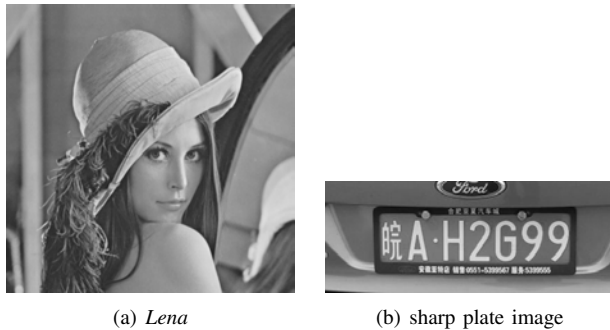


Fig. 3: Images used in our simulation experiment.

introduced a new model of spatially random distribution of image noise and a new smooth constraint of latent image. In [6], [10], the authors proposed to add one prediction (or selection) step to enhance the large scale edges to improve the performance. Based on the same idea, Xu *et al.* [8] introduced an unnatural ℓ_0 sparsity prior, and the sparsity function used in their algorithm has the similar effect with edge prediction. In this strategy, the edge prediction is critical for the deblurring performance.

Another alternative is to introduce more complicated prior, such as framelet [16], [17] and transparency information [18], [19]. Motivated by the great success of sparse representation in the field of image processing and computer vision [20], [21], the sparsity on a learned over-complete dictionary is used as the prior of sharp image in Hu's work [22]. For the special blurred document, Chen [23] and Cho [9] introduced a well-designed prior which is computed by text detection algorithm [24], [25]. However, both of these two methods require that the image is big enough and the background is not very complex. Goldstein *et al.* [26] proposed to estimate the power spectrum of the blur kernel with a spectral whitening formula. Liu *et al.* [27] introduced a convex kernel regularizer to the prevalent nonblind deconvolution methods, which showed impressive performance in their paper.

There are also other researchers resorting to more information about the latent sharp image. Zhang *et al.* [28], Yuan *et al.* [29] and Hu *et al.* [30] proposed to use a pair of images to estimate a more accurate blur kernel, which can reduce the deblurring artifacts. Tai *et al.* attempted to solve the deblurring problem by constructing a special camera hardware which can record an auxiliary lower resolution but higher frame-rate video [1]. However, the requirement of multi-observation method or hardware is infeasible in many real applications [31], [32].

The limits of MAP framework are obvious. Firstly, MAP with simple gradient prior cannot guarantee that the true solution is available in most area of images. Secondly, when the kernel size is very large, usually insufficient edges can be filtered out in the blurred image, which significantly affects final result.

B. Marginalization methods

The marginalization methods are based on the observation that maximizing $p(k|B)$ usually leads to a more robust and

accurate kernel even under a weak prior of sharp image [11], [13], [14], [33]. These methods firstly estimate the kernel by expectation maximization (EM) algorithm, and then apply NBID only once. Wang *et al.* [14] combined the marginalization method and large scale step edge prediction technique to improve the robustness of deblurring algorithm.

However, it can be proved theoretically that the max-marginalization method can only handle small kernel situations (*i.e.*, the size of kernel is much smaller than the size of observed image). In fact, in our scenario, the kernel size even reaches one-third the size of the blurred image. Another drawback of the marginalization method is that the computational complexity grows rapidly by introducing the EM algorithm.

C. Parametric kernel estimation methods

Most of the algorithms mentioned above attempt to estimate a general kernel with the only constraint that every element of kernel is nonnegative. However, in real world, several common blur kernels are parametric, such as blur caused by moving at a constant speed and out-of-focus blur [12]. The blur estimation problem can be reduced to a parameter estimation problem which is much more tractable. Parametric blur estimation algorithms utilize the property that linear uniform blur kernel's spectrum is sinc-like function which is distinctive from natural image [12], [34]. Oliveira *et al.* assumed nature image to be approximately isotropic, which is valid for natural image with large size. However, for small image, the spectrum is heavily dependent on the content of the image such as large scale edge.

For non-uniform deblurring, the kernel estimation is a thornier problem because a strict non-uniform kernel has too many degrees of freedom. To simplify the estimation of kernel, the non-uniform blurring is typically assumed to be caused by projection transform [35]–[37]. Whyte *et al.* [35] assumed that the blur from camera shake is mostly due to the 3D rotation of camera, which could be approximated by roll, yaw and pitch. In a similar way, Gupta *et al.* [36] reduced the motion of camera into 3D subspace: roll and x, y-translations. In a recent work, Zheng *et al.* [37] estimated the normal vector of the plane in the camera scene and the camera's motion direction to handle the forward or backward motion blur.

For over-speed license plate deblurring, the size of blur kernel is very large, even reaching one-third of the size of blurred image, which poses great challenges to both the MAP and marginalization methods. To tackle this problem, we adopt the blur kernel parameter estimation method (angle and length). For angle estimation, our scheme makes use of the relationship between the kernel angle and sparse representation coefficients. For length estimation, we exploit the fact that the behavior of power spectrum is significantly affected by the length of kernel in Fourier domain. The major advantage of our method is that the proposed scheme can handle large motion blur even when the license plate is unrecognizable by human, which makes our approach promising in real applications.

III. ESTIMATION OF BLUR KERNEL

Generally, the blur kernel is determined by the relative motion between the moving vehicle and static surveillance

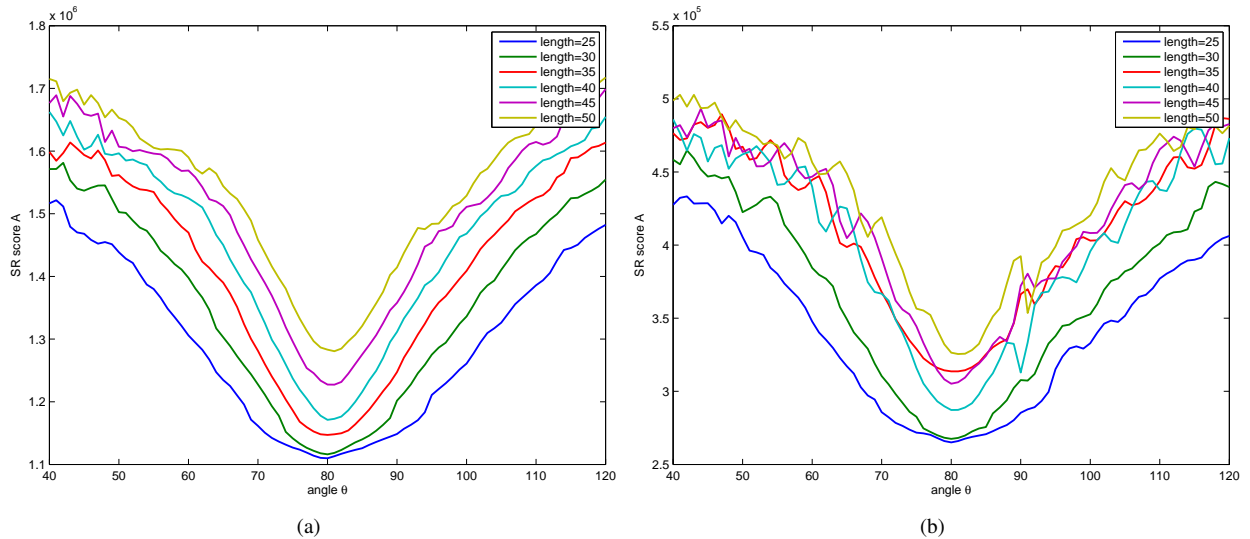


Fig. 4: Relation between A and θ under different length settings, (a) *Lena*; (b) real license plate image. The ground truth setting is $(\theta = 80^\circ, l = 35)$.

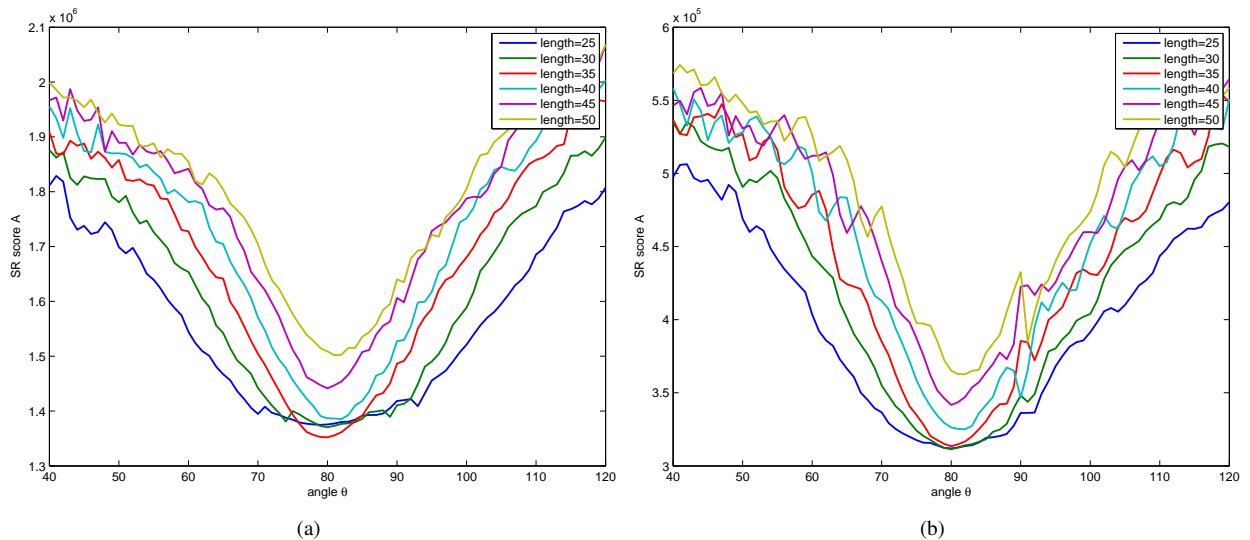


Fig. 5: Relation between A and θ under different length settings with Gaussian noise ($\sigma=5$), (a) *Lena*; (b) real license plate image. The ground truth setting is $(\theta = 80^\circ, l = 35)$.

camera during the exposure time. When the exposure time is very short and the vehicle is moving very fast, the motion can be regarded as linear and the speed can be considered as approximately constant. In such cases, the blur kernel of license plate image can be modeled as a linear uniform kernel with two parameters: *angle* and *length* [15]. In the following Section III-A, we introduce how to utilize sparse representation on over-complete dictionary to evaluate the angle of kernel robustly. After the angle estimation, in Section III-B, frequency domain-based method is proposed to estimate the length of kernel. At last, we summarize our algorithms in details in Section III-C. Fig. 2 shows the overall flow chart of our proposed scheme.

A. Angle estimation of linear uniform kernel

Sparsity on learned over-complete dictionary as the prior of sharp image has been well discussed [21], [22], however,

sparse representation has received little attention in parameter inference.

In fact, parameter estimation also corresponds to an optimization problem in a Bayesian view. For angle estimation, it can be regarded as solving the following problem:

$$(\vartheta, I) = \operatorname{argmin}_{\theta, I} \left\{ -\log p(I) + \frac{\lambda}{2} \|k_\theta * I - B\|_F^2 \right\} \quad (3)$$

where B is the blurred image, I denotes the latent image to be recovered, k_θ is the linear uniform motion kernel determined by angle θ (ignore length here), and $p(I)$ is the prior of the sharp image.

By introducing sparse representation, in our angle estima-

tion algorithm, we attempt to solve:

$$\begin{aligned} \vartheta &= \operatorname{argmin}_{\theta} \sum |\alpha_i| \\ \text{s.t.} \quad \Omega_i X &= D\alpha_i \\ X &= \operatorname{argmin}_I \{ |I|_{TV} + \frac{\lambda}{2} |k_{\theta} * I - B|_F^2 \} \end{aligned} \quad (4)$$

where D is pre-learned over-complete dictionary on the sharp license plate images, Ω_i is the patch extraction operator, and α_i is the sparse representation coefficients of the i th patch. The physical meaning of Eq. (4) is that the angle we intend to estimate is the one with which the recovered sharp image has the sparsest representation.

The key to solve Eq. (4) is to estimate the gradient $\frac{\partial \sum |\alpha_i|}{\partial \theta}$. However, it is difficult to directly solve such a two-layer optimization problem. In order to investigate the relation between $\sum |\alpha_i|$ and the variable θ , we decompose Eq. (4) into two simpler sub-problems. For a given parameter pair (θ, l) , we first solve the following optimization problem,

$$X = \operatorname{argmin}_I \{ |I|_{TV} + \frac{\lambda}{2} |k_{\theta} * I - B|_F^2 \} \quad (5)$$

Then the sparse representation coefficient $\sum |\alpha_i|$ can be computed by solving:

$$\begin{aligned} \min_{\alpha_i} \sum |\alpha_i| \\ \text{s.t.} \quad \Omega_i X &= D\alpha_i \end{aligned} \quad (6)$$

Here, for simplicity, we define $A = \sum |\alpha_i|$. Therefore, $A(\theta, l)$ can be regarded as a function of kernel parameters (θ, l) . In order to explore the property of $A(\theta)$ (ignore l here), we have done some experiments on two example images: *Lena* and a real sharp license plate image (shown in Fig. 3). Firstly, we blur the sharp *Lena* and license plate image with a linear uniform motion blur kernel with an angle of 80 degrees and a length of 35 pixels ($\theta = 80^\circ, l = 35$). In Fig. 4, we plot the relation between A and θ under different length settings for *Lena* and the license plate, respectively. In Fig. 5, we add Gaussian white noise to the blurred image (the standard variance $\sigma = 5$). We can see that no matter whether noise exists or not in the observed images, the relation between A and θ shows a quasi-convex curve on both natural and license plate images. Under different length settings, the minimum of A is achieved when θ corresponds to the ground truth angle.

Furthermore, we explore this characteristic of sparse representation on three plate images. Each image is blurred by a series of linear motion blur kernels (angle varying in the range $[0^\circ, 90^\circ]$ under three length settings) with Gaussian noise. The angle that corresponds to the smallest score A is regarded as our estimated angle. Fig. 6 reports the accuracy assessed by root mean squared error (RMSE) (in degree) over 5 runs under different ground truth kernel settings. The errors of angle estimation stay in a low level and are essentially independent of the ground truth angles.

The main difficulty in solving the optimization by Eq. (4) is that the gradient cannot be calculated efficiently. However, the quasi-convex property from the sparse representation brings a great improvement on this optimization problem. Even though the gradient $\frac{\partial A}{\partial \theta}$ has no closed form, we can estimate the

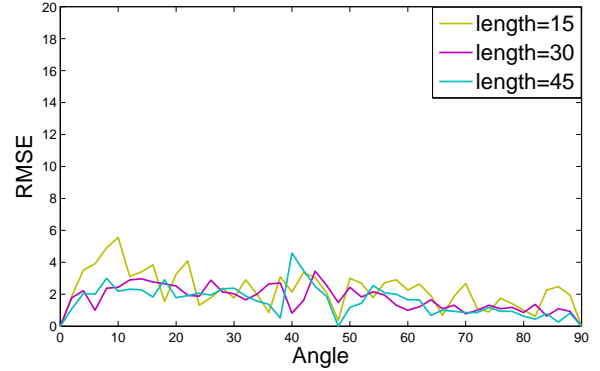


Fig. 6: RMSE of angle estimation. The noise level is $\sigma = 5$.

gradient by computing Eq. (5) and (6) twice. Then we use the gradient descent method to find the optimization value. In Fig. 4 and Fig. 5, we can see that there are several outliers on the curves. In order to reduce the effect of outliers, the step of gradient descent should not be too small. However, large step may lead to the degradation of accuracy. So we propose a two-step coarse-to-fine angle estimation algorithm, which will be elaborated on in Section III-C.

As mentioned above, the sparse representation score A provides us a useful clue to determine the angle of the blur kernel. In addition, there are also some other blurriness metrics which were proposed recently. As a typical example, Liu *et al.* proposed a complex metric for motion deblurring, which combined several popular image quality assessment measures [38]. We first blur Fig. 3(b) with kernel ($\theta = 80^\circ, l = 35$) to obtain the blurred image, which is then deblurred with a series of linear uniform kernels using Eq. (5). For each deblurred image, the corresponding Liu's measure can be calculated. Fig. 7(a) shows the relation between Liu's metric and the kernel parameters, where higher value means better deblurring performance. Comparing with Fig. 4(b), under different length settings, the curves show distinct trends. Especially when the length setting is shorter than the ground truth (see green and blue curve in Fig. 7(a)), Liu's metric fails to achieve the peak value around the ground truth ($\theta = 80^\circ$). Besides, there are many statistically justified metrics as well. Here, we adopt the classical Steins unbiased risk estimate (SURE). The result of SURE in Fig. 7(b) is obtained by Monte-Carlo algorithm, in which each point is computed using 10 examples [39], [40]. The SURE also shows the similar quasi-convex properties. However, the SURE keeps in low value in large range around the ground truth (see blue, green and red curves in Fig. 7(b)), which makes it difficult to determine the optimal angle as the final estimation result.

Different from the general natural scene images, license plate images usually only contain some specific characters, such as English letters and digits. Therefore, license plate images are characterized by very particular and limited patterns, which can be well learned by sparse representation. In this paper, our dictionary is trained on sharp license plate images. Hence, the prior knowledge about license plate images is already embedded in the over-complete dictionary. In this

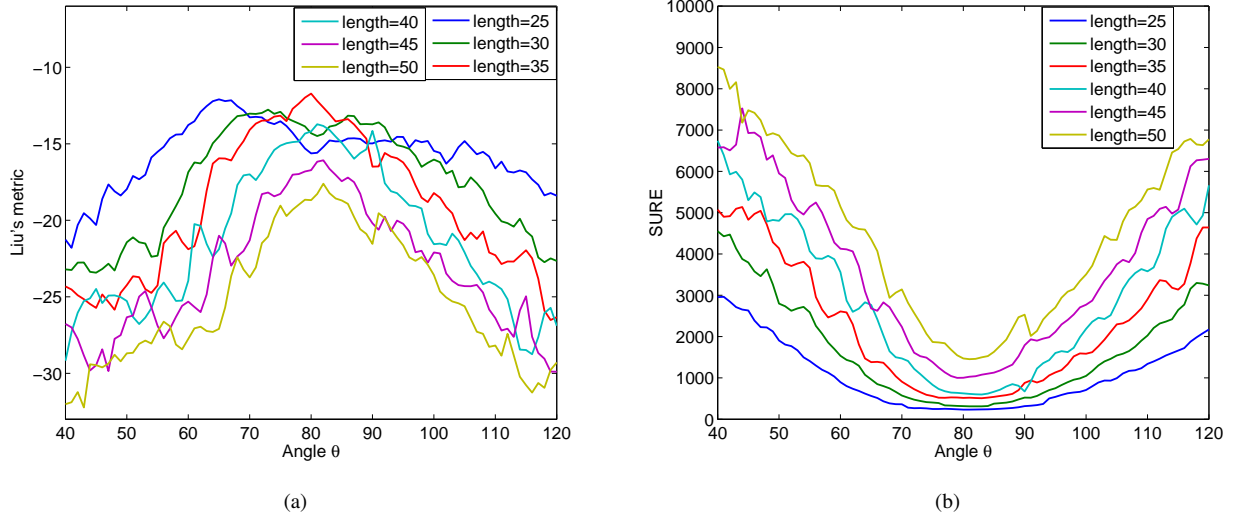


Fig. 7: Performance of Liu's metric and SURE under different length settings for Fig. 3(b). (a) Liu's metric; (b) SURE obtained by Monte-Carlo algorithm. The ground truth setting is ($\theta = 80^\circ$, $l = 35$).

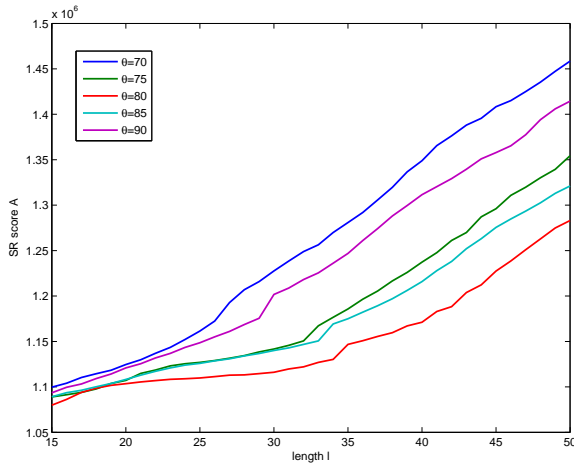


Fig. 8: Relation between A and l on *Lena* under different angle settings. The ground truth setting is ($\theta = 80^\circ$, $l = 35$).

view, the prior used in this paper is more specific and adaptive, which is beneficial to angle estimation.

Sparse representation coefficients show great potential in the angle estimation of linear uniform kernel. A natural extension is to apply it to the length inference. However, sparse representation coefficients do not show such quasi-convex characteristic with the variation of length. As shown in Fig. 4(a), Fig. 4(b), and Fig. 5(b), A achieves the minimum when l is set as 25, while the ground truth of length is 35. Furthermore, in Fig. 8, we plot the relation between A and l when the angle is fixed, where the sparse representation coefficients show the monotonic increasing property with the increase of l . In other words, if we use the sparsity on over-complete dictionary as prior, the result favors a shorter kernel no matter whether the angle is correct or not.

B. Length estimation of linear uniform kernel

Once the direction of motion has been fixed, we can rotate the blurred image to make this direction horizontal. Then the uniform linear motion blur kernel has the form as below:

$$k(x, y) = \begin{cases} \frac{1}{L} & x = 0, 1, \dots, L-1; y = 0 \\ 0 & \text{otherwise} \end{cases} \quad (7)$$

The magnitude of the frequency response of $k(x, y)$ on horizontal direction is given by the following equation:

$$|F_k(v)| \propto \frac{\sin(\frac{L\pi v}{N})}{L \sin(\frac{\pi v}{N})} \quad v = 0, 1, \dots, N-1 \quad (8)$$

where N is the size of blurred image in pixel. Given two successive zero points v_1, v_2 of $F_k(v)$, it is easy to obtain that:

$$L = \frac{N}{|v_1 - v_2|} \quad (9)$$

Thus, the core of length estimation is to estimate the distance between two adjacent zero points of frequency response of kernel. In frequency domain, the uniform blur model can be written as:

$$F_B(u, v) = F_k(u, v)F_I(u, v) + F_G(u, v) \quad (10)$$

where F denotes the Fourier transform operator.

We can find that the zero points of F_k is also the zeros points of F_B without considering noise. In most of real situations, it is difficult to directly search zero points in the frequency response of observed image. Due to noise, the zero points of F_k may not exactly denote the zero points of F_B ; however, the magnitude of F_B around zero points still can be distinguished from other points as the power spectrum of natural images along lines through the origin point obeys the following power-law [41] [42]

$$|F_I(\omega)| \propto |\omega|^{-\gamma} \quad (11)$$

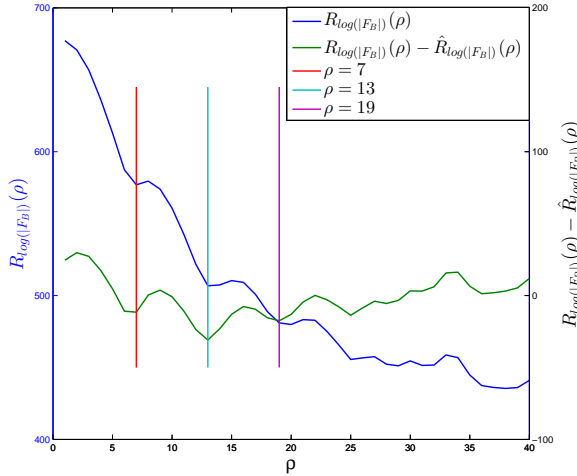


Fig. 9: Relation between $R_{\log|F_B|}(\rho) - \hat{R}_{\log|F_B|}(\rho)$ and $R_{\log|F_B|}(\rho)$ of blurred plate image in real scene on the estimated angle θ .

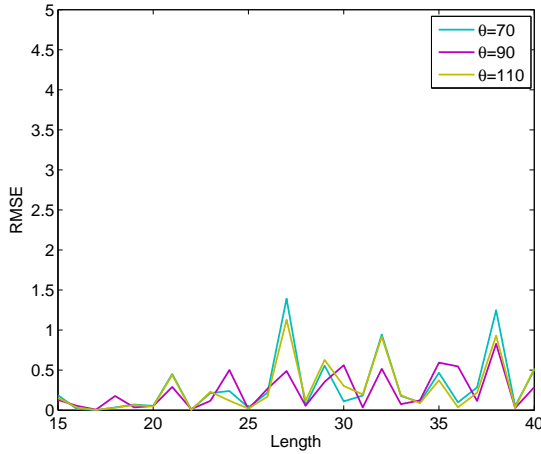


Fig. 10: RMSE of length estimation.

where the value of γ may vary with the angle of lines due to the presence of large scale edge. Next, we exploit the power-law and Radon transform to infer the distance between two adjacent zero points of $|F_k|$.

Radon transform is an integral transform that collects the sum of a function over straight lines. Radon transform result can be represented by the angle between horizontal axes α and the distance to the origin point ρ [43]. For BID, Radon transform is proposed to estimate the motion blur kernel [12], especially when the observed image is corrupted by noise [44], [45]. In our length estimation algorithm, we adopt the modified Radon transform which only considers the center area of blurred image [12]. The modified Radon transform is defined as:

$$R_f(\alpha, \rho) = \int_{-d}^{+d} f(\rho \cos \alpha - x \sin \alpha, \rho \sin \alpha + x \cos \alpha) dx \quad (12)$$

where f is a general 2D function to be Radon transformed. For the blurred images, under weak noise assumption ($F_G \approx 0$),

Algorithm 1 Coarse angle estimation

Input: Blurred image B , step Δ , initial angle θ_0 , a moderate length l , $k = 0$

- 1: **while** not converged **do**
- 2: Generate uniform linear kernel $k_{l, \theta_k}, k_{l, \theta_k - \Delta}, k_{l, \theta_k + \Delta}$
- 3: Solve Eq. (5) with kernels $k_{l, \theta_k}, k_{l, \theta_k - \Delta}, k_{l, \theta_k + \Delta}$, get deblurred images $I_{l, \theta_k}, I_{l, \theta_k - \Delta}, I_{l, \theta_k + \Delta}$
- 4: Solve Eq. (6) with $I_{l, \theta_k}, I_{l, \theta_k - \Delta}, I_{l, \theta_k + \Delta}$, get $A_{l, \theta_k}, A_{l, \theta_k - \Delta}, A_{l, \theta_k + \Delta}$
- 5: **if** $A_{l, \theta_k} == \min(A_{l, \theta_k}, A_{l, \theta_k - \Delta}, A_{l, \theta_k + \Delta})$
- 6: converged and return
- 7: **elseif** $A_{l, \theta_k - \Delta} == \min(A_{l, \theta_k}, A_{l, \theta_k - \Delta}, A_{l, \theta_k + \Delta})$
- 8: $\theta_k \leftarrow \theta_k - \Delta$
- 9: **else**
- 10: $\theta_k \leftarrow \theta_k + \Delta$
- 11: **end while**

Output: θ_k

we have

$$R_{\log|F_B|}(\alpha, \rho) \approx R_{\log|F_I|}(\alpha, \rho) + R_{\log|F_k|}(\alpha, \rho) \quad (13)$$

Based on the assumption of power-law, for one fixed angle α , $R_{\log|F_I|}(\rho)$ is also a polynomial function. We use a three order polynomial function to fit $R_{\log|F_B|}(\rho)$

$$\hat{R}_{\log|F_B|}(\rho) = a\rho^3 + b\rho^2 + c\rho + d \quad (14)$$

The local minimums of $R_{\log|F_B|}(\rho) - \hat{R}_{\log|F_B|}(\rho)$ correspond to the zeros points of $R_{\log|F_k|}(\rho)$, as shown in Fig. 9. Through detecting the distance between two consecutive local minimums of $R_{\log|F_B|}(\rho) - \hat{R}_{\log|F_B|}(\rho)$, we can then estimate the length of kernel by Eq. (9).

We report the performance of the proposed length estimation method in Fig. 10. The estimation error is also assessed by RMSE (in pixel) on three plate licence images with size of about 200×400 . The estimation error stays in low level under three angle settings with the variation of length.

C. Summary of proposed scheme

In the angle estimation stage, we adopt a two-step coarse-to-fine framework. In the first step, the quasi-convex property is utilized to find the initial best angle under coarse granularity for any moderate length. The algorithm is summarized in Algorithm 1. In general, it only takes several iterations for Algorithm 1 to converge. Once the initial estimated angle is obtained, we perform the fine angle estimation. In Algorithm 1, all the operations are applied on a fixed length; whereas the fine estimation of angle is implemented on a multi-length setting, the details of which can be found in Algorithm 2.

In both Algorithms 1 and 2, it is critical to solve Eq. (5) and (6). The over-complete dictionary D is pre-trained on the sharp license plate images. Both dictionary learning and Eq. (6) are solved with Lee's feature-sign algorithm [46]. For Eq. (5), there are many successful algorithms [47]. In this paper, we adopt the popular split-Bregman method [48]. We

Algorithm 2 Fine angle estimation

Input: Blurred image B , the output of Algorithm 1 θ , a moderate length l

- 1: Generate a series of pair (θ_i, l_i) (responding kernel k_i) that center about (θ, l)
- 2: Solve Eq. (5) with kernel k_i , get I_i
- 3: Solve Eq. (6) with I_i , get A_i
- 4: Sort A_i by increasing order
- 5: Get the top- k A_i and the corresponding θ_i

Output: The average of top- k θ_i

Algorithm 3 Non-blind image deblurring

Input: Blurred image B , kernel k , the balance parameter λ

- 1: Initialize the Bregman multipliers b_x, b_y and Bregman parameter ϵ
- 2: **while** not converged **do**
- 3: $\operatorname{argmin}_I \{ \frac{\lambda}{2} |k * I - B|_F^2 + \frac{\epsilon}{2} |d_x - \nabla_x I - b_x|_F^2 + \frac{\epsilon}{2} |d_y - \nabla_y I - b_y|_F^2 \}$, solved by gradient descent method
- 4: $\operatorname{argmin}_{d_x} \{ |d_x| + \frac{\epsilon}{2} |d_x - \nabla_x I - b_x|_F^2 \}$, solved by shrinkage operator
- 5: $\operatorname{argmin}_{d_y} \{ |d_y| + \frac{\epsilon}{2} |d_y - \nabla_y I - b_y|_F^2 \}$, solved by shrinkage operator
- 6: Update Bregman multiplier
- 7: $b_x \leftarrow b_x + \nabla_x I - d_x$
- 8: $b_y \leftarrow b_y + \nabla_y I - d_y$
- 9: **if** reach the max-iteration
- 10: converged and return
- 11: **endif**
- 12: **end while**

Output: The recovered image I

rewrite problem (5) into the following form:

$$\begin{aligned} & \operatorname{argmin}_I \{ |d_x| + |d_y| + \frac{\lambda}{2} |k * I - B|_F^2 \} \\ \text{s.t.} \quad & d_x = \nabla_x I \\ & d_y = \nabla_y I \end{aligned} \quad (15)$$

The detail of solving Eq. (15) (or equally Eq. (5)) is listed in Algorithm 3.

In the angle estimation stage, the NBID algorithm does not involve complicated prior information. The reason is that complicated prior usually incurs high computational complexity. The length estimation scheme is summarized in Algorithm 4 and its principle can be found in Section III-B.

After obtaining the parameters of blur kernel, the final non-blind deblurring is done with the NBID algorithm proposed by Whyte *et al.* [49].

IV. EXPERIMENTAL RESULTS AND DISCUSSION

In this section, we compare the proposed method with several existing state-of-the-art deblurring methods on real blurred plate images. The parameter settings and computational complexity are also discussed in detail.

Algorithm 4 Length estimation

Input: Blurred image B , the output of Algorithm 2 θ

- 1: Extend B into a square image (the size is $N \times N$) and calculate logarithm of frequency magnitude of B denoted by $\log(|F_B|)$
- 2: Apply modified Radon transform on $\log(|F_B|)$ over the angle θ , $R_{\log(|F_B|)}(\rho)$ denotes the result
- 3: Fit $R_{\log(|F_B|)}(\rho)$ with three order polynomial function through least square error method, the fitting result is $\hat{R}_{\log(|F_B|)}(\rho)$
- 4: Get the distance of two consecutive local minimums of $R_{\log(|F_B|)}(\rho) - \hat{R}_{\log(|F_B|)}(\rho)$ denoted by d
- 5: Get the estimated length by $L = \frac{N}{d}$

Output: The length of kernel L

A. Experimental data

All the experimental data used in our experiments are captured in real scenarios. The static license plate images that are used to learn the over-complete dictionary are taken by Nikon Coolpix P7000 under different scales from the front view. One sample of sharp license plate images is shown in Fig. 3(b). For the blurred license plate images, we capture the images by fixing the camera (Canon 7D) on the tripod which is put on footbridge. Fig. 1 shows a blurred image degraded by motion blur in real scene. The region of licence plate with size of about 100×200 pixels is extracted from image in advance, and our scheme is only applied on such regions. In our kernel estimation procedure, sparse representation plays a key role in angle estimation. In the past years, several powerful dictionary learning methods have been proposed [46], [50], [51]. Lee's algorithm is used in our dictionary learning stage [46]. From the sharp license plate images we take, ten thousand patches with the size of 8×8 are extracted, and the other parameters' setting follows the proposal of [46]. Then a dictionary with 512 atoms can be obtained.

B. Implementation of our scheme

For the Eq. (5), λ is set as 500. We find that λ can vary in a wide range without notable impact on the final deblurred results. In the coarse angle estimation stage, the step Δ is 5 considering the robustness and computing complexity. Another parameter is the starting angle θ_0 . For over-speed car license plate blur, the angle of motion kernel is usually in the range [40, 140]. So we set θ_0 as 90° . For Eq. (6), sparse representation is applied to overlapped patches. The patches with the size of 8×8 are sampled every 6 pixels along horizontal and vertical axes. And the sum of absolute value of all patches' sparse representation coefficients is regarded as the final score.

In the fine angle estimation stage, centering at the output θ of the last module, we generate a series of parameter pairs (θ_i, l_i) , where the length l_i lies in the range [25, 49] with step size 3, and θ_i lies in the range $[\theta - 10, \theta + 10]$ with step size 5. That means we have 45 images to apply NBID and sparse coding algorithm. Since this process is highly separated, parallel algorithm can be designed for it. Then we select

TABLE I: Recognition rate of different BID methods

BID schemes	Recognition rate
Unprocessed images	9.10%
NSBD [52]	18.18%
TPISD/USR [8], [10]	43.18%
Proposed algorithm	79.55%

six angles corresponding to the smallest sparse representation scores. The average of the six angles is taken as the final angle. In the angle estimation stage, deconvolution is done on each RGB channel independently. Sparse representation is only implemented on the luminance channel considering the computing complexity.

Our algorithm is implemented with MATLAB script without optimization and runs on a workstation with Intel Xeon CPU@2.40GHz and 32GB RAM.

C. Evaluation of the proposed algorithm

For the blurred images we captured in real scenario, the ground truth is unavailable. In order to test the validity of our proposed algorithm, we deblur the captured images with different linear kernels which have small bias on angle or length compared with our estimated parameters. Figs. 11, 12 and 13 demonstrate that our estimated results are exact or near the best parameters on three examples under different blur levels. The plate images become recognizable after deblurring under our estimated parameter settings.

We compare our proposed scheme with four state-of-the-art blind image deblurring methods: 1) NSBD [52]; 2) Xu's methods (TPISD [10]/USR [8]); 3) FSR [17]; 4) HQMD [7]. We use the source codes of those comparison methods downloaded from the authors' websites. NSBD [52] and FSR [17] do not need edge detection or equivalent operations. USR [8] and HQMD [7] are based on edge detection or prediction. Xu's method [8] requires the size of image be larger than 200×200 in pixel. When the height of our observed image is smaller than 200, an extra super-resolution is applied before applying Xu's BID method. After obtaining the recovered sharp image, we acquire the final restored image by down-sampling to the raw size.

Fig. 14 and Fig. 15 show the deblurring performance of our scheme and other comparing algorithms under different situations. In most cases, the proposed method achieves the best performance improvement and successfully improves the plate image from unrecognizable to recognizable. The second and third images of Fig. 14, the first and second images of Fig. 15 show the same great improvement on semantic recognition. It can be observed that in real scene and very large blur condition, deblurring artifact is unavoidable no matter which BID algorithm is chosen. However, in our scheme, the artifact does not damage the semantic information on most images. At the same time, our scheme demonstrates the best robustness.

To quantitatively demonstrate the gain, we also evaluate the deblurring performance with recognition rates of license plate in the character level. We train a support vector machine with radial basis function kernel (RBF-SVM) as classifier after

TABLE II: Running time of different methods

BID schemes	Running time(s)
TPISD/USR (optimized by C++ and CUDA) [8], [10]	45.68
NSBD [52]	11.84
FSR [17]	135.23
HQMD (optimized by C++) [7]	736.89
Proposed algorithm	347.95

resizing every sharp character into a fixed size. There are totally 240 licence plate images in the training dataset. All the parameters of SVM follow the suggestion of *LIBSVM* [53]. In the test stage, the pre-trained SVM is applied on 9 licence plate images captured in real cases. The performance improvement on recognition rate is shown in Table I. Apparently, the recognition rate is notably improved after deconvolution and the proposed algorithm achieves the highest recognition rate.

In our scheme, the fine angle estimation stage is the most time consuming. Under our parameter setting, it needs to conduct sparse representation and NBID 45 times. Therefore, the time complexities of our scheme are $O(MN)$ (M is the number of iteration in each sparse representation and NBID, and N is the image size). Table II shows the running time of the five different blind image deblurring algorithms on a real blurred plate image with size of about 200×300 .

D. Discussion

Blur kernel estimation can be regarded as searching the best solution in a large blur kernel space. By constraining the blur kernel, the search range can be greatly reduced, which can significantly improve the robustness of blur kernel estimation. The experimental results demonstrate that such constraints on blur kernels are very effective. For blind deblurring of license plate images, we pay more attention on the semantic content of images, *i.e.*, we aim to recognize the blurred plate license image after deblurring processing. Even though there are still some artifacts in the final deblurred result, most of the semantic information has been recovered.

V. CONCLUSION

In this paper, we propose a novel kernel parameter estimation algorithm for license plate from fast-moving vehicles. Under some very weak assumptions, the license plate deblurring problem can be reduced to a parameter estimation problem. An interesting quasi-convex property of sparse representation coefficients with kernel parameter (angle) is uncovered and exploited. This property leads us to design a coarse-to-fine algorithm to estimate the angle efficiently. The length estimation is completed by exploring the well-used power-spectrum character of natural image.

One advantage of our algorithm is that our model can handle very large blur kernel. As shown by experiments in Section IV, for the license plate that cannot be recognized by human, the deblurred result becomes readable. Another advantage is that our scheme is more robust. This benefits from the compactness of our model as well as the fact that our method does not make strong assumption about the content of image such as edge or isotropic property.

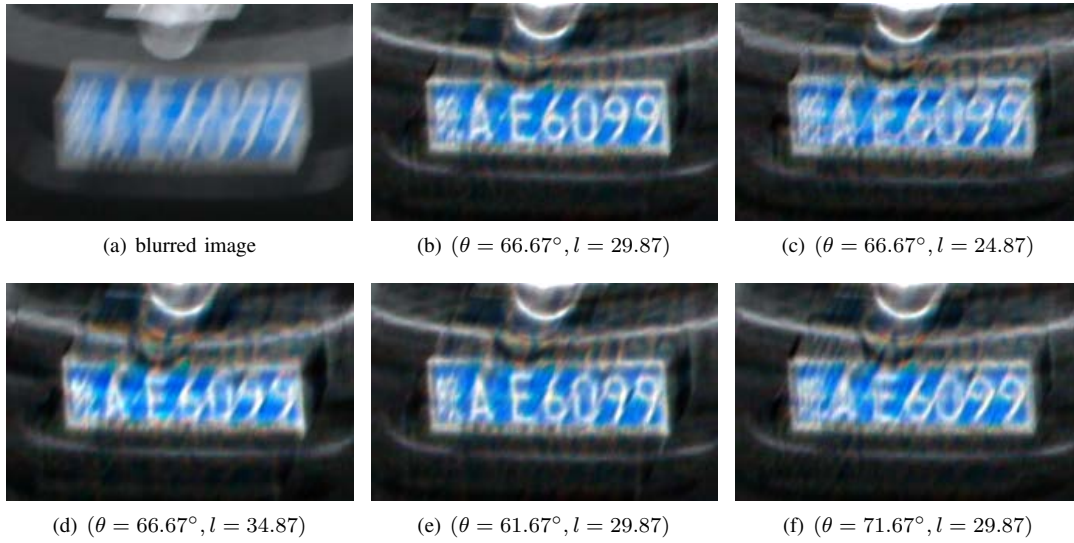


Fig. 11: Middle blur example. The image size is 224×140 , and our estimated kernel parameters are $(\theta = 66.67^\circ, l = 29.87)$. Top-left is the observed license plate image. Top-middle is our recovered result. The other four images are the results acquired by modifying the kernel parameters with a small bias on the estimated angle or length.

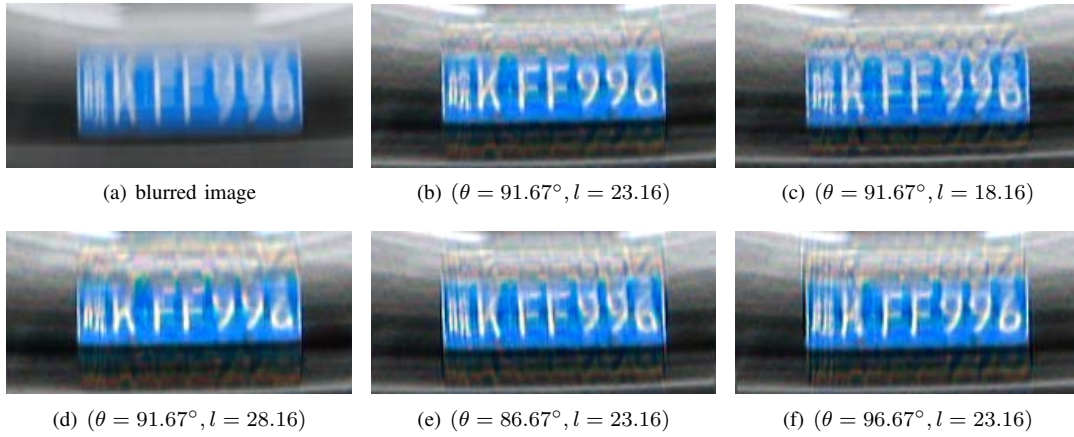


Fig. 12: Small blur example. The image size is 220×104 , and the estimated kernel parameter are $(\theta = 91.67^\circ, l = 23.16)$. In this paper, we regard this situation as small blur, because we are still able to recognize the number of this plate. However in the other paper, this is large blur considering the size of image.

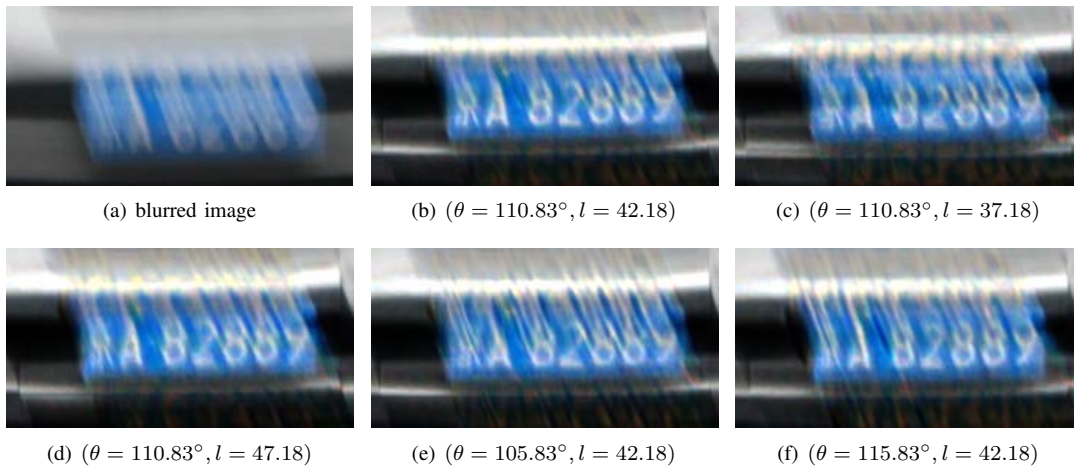


Fig. 13: Large blur example. The size of image is 232×120 . Top-middle is our result and the responding kernel parameter is $(\theta = 110.83^\circ, l = 42.18)$. In this situation, human almost cannot recognize the plate. After deblurring, we can figure out the first Chinese character effortlessly, as shown in (b).

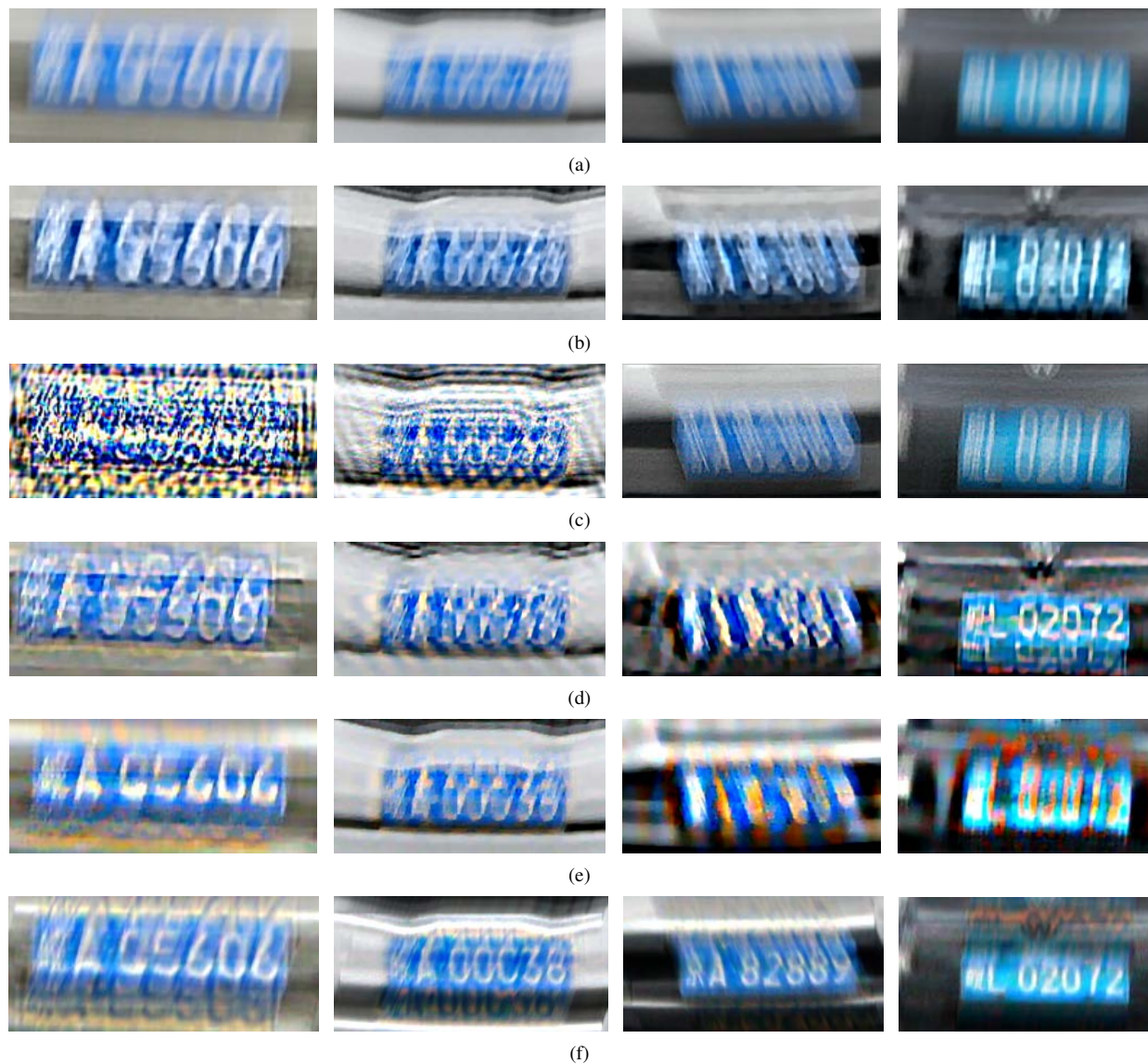


Fig. 14: Performance comparison in real situations: (a) blurred images, (b) NSBD [52], (c) FSR [17], (d) HQMD [7], (e) TPISD [10]/USR [8], (f) our method.

In our scheme, we only use very simple and naive NBID algorithm. And there is still obvious artifact in the deblurred results. However, for many practical applications, people are more interested in identifying the semantics of the image. From this view, our scheme brings great improvement on the license plate recognition.

REFERENCES

- [1] Y.-W. Tai, H. Du, M. Brown, and S. Lin, "Correction of spatially varying image and video motion blur using a hybrid camera," *IEEE Transactions on Pattern Analysis and Machine Intelligence (TPAMI)*, vol. 32, no. 6, pp. 1012–1028, Jun 2010.
- [2] W. Zhou, Y. Lu, H. Li, Y. Song, and Q. Tian, "Principal visual word discovery for automatic license plate detection," *IEEE Transactions on Image Processing (TIP)*, vol. 21, no. 9, pp. 4269–4279, 2012.
- [3] W. Zhou, Y. Lu, H. Li, Y. Song, and Q. Tian, "Spatial coding for large scale partial-duplicate web image search," in *Proceedings of the 18th ACM international conference on Multimedia*, Oct 2010, pp. 511–520.
- [4] W. Zhou, H. Li, R. Hong, Y. Lu, and Q. Tian, "Bsift: toward data-independent codebook for large scale image search," *IEEE Transactions on Image Processing (TIP)*, vol. 24, no. 3, pp. 967–979, 2015.
- [5] W. Zhou, M. Yang, H. Li, X. Wang, Y. Lin, and Q. Tian, "Towards codebook-free: Scalable cascaded hashing for mobile image search," *IEEE Transactions on Multimedia (TMM)*, vol. 16, no. 3, pp. 601–611, 2014.
- [6] S. Cho and S. Lee, "Fast motion deblurring," *ACM Transactions on Graphics (TOG)*, vol. 28, no. 5, pp. 145:1–145:8, Dec 2009.
- [7] Q. Shan, J. Jia, and A. Agarwala, "High-quality motion deblurring from a single image," *ACM Transactions on Graphics (TOG)*, vol. 27, no. 3, pp. 73:1–73:10, 2008.
- [8] L. Xu, S. Zheng, and J. Jia, "Unnatural ℓ_0 sparse representation for natural image deblurring," in *Proceedings of IEEE Conference on Computer Vision and Pattern Recognition (CVPR)*, Jun 2013, pp. 1107–1114.
- [9] H. Cho, J. Wang, and S. Lee, "Text image deblurring using text-specific properties," in *Proceedings of European Conference on Computer Vision (ECCV)*, Oct 2012, pp. 524–537.
- [10] L. Xu and J. Jia, "Two-phase kernel estimation for robust motion deblurring," in *Proceedings of European Conference on Computer Vision (ECCV)*, Sep 2010, pp. 157–170.
- [11] A. Levin, Y. Weiss, F. Durand, and W. T. Freeman, "Understanding blind deconvolution algorithms," *IEEE Transactions on Pattern Analysis and Machine Intelligence (TPAMI)*, vol. 33, no. 12, pp. 2354–2367, 2011.
- [12] J. Oliveira, M. Figueiredo, and J. Bioucas-Dias, "Parametric blur estimation for blind restoration of natural images: linear motion and out-of-focus," *IEEE Transactions on Image Processing (TIP)*, vol. 23, no. 1,

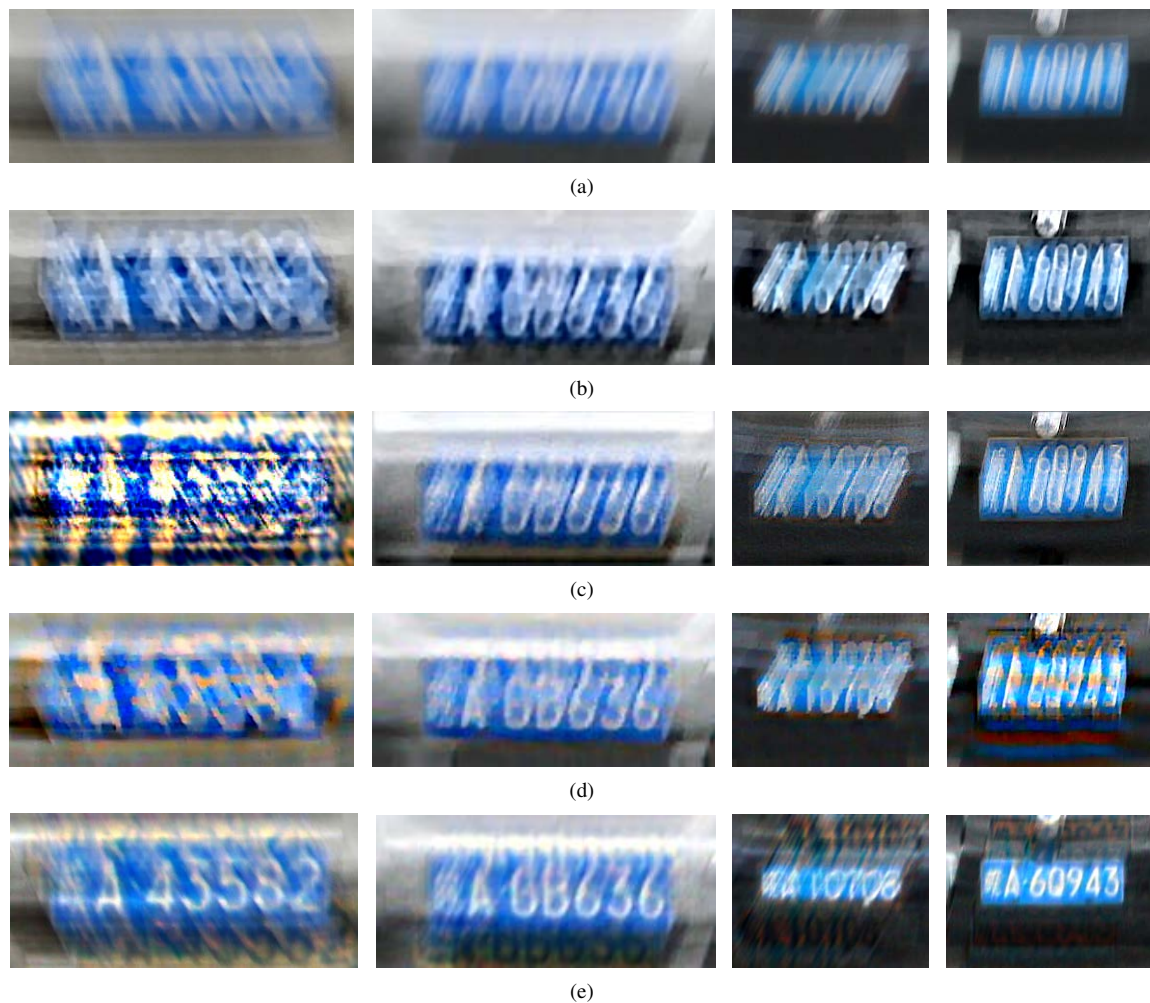


Fig. 15: More performance comparison in real situations: (a) blurred images, (b) NSBD [52], (c) FSR [17], (d) TPISD [10]/USR [8], (e) our method.

- pp. 466–477, Jan 2014.
- [13] R. Fergus, B. Singh, A. Hertzmann, S. T. Roweis, and W. T. Freeman, “Removing camera shake from a single photograph,” *ACM Transactions on Graphics (TOG)*, vol. 25, no. 3, pp. 787–794, 2006.
- [14] C. Wang, Y. Yue, F. Dong, Y. Tao, X. Ma, G. Clapworthy, H. Lin, and X. Ye, “Nonedge-specific adaptive scheme for highly robust blind motion deblurring of natural images,” *IEEE Transactions on Image Processing (TIP)*, vol. 22, no. 3, pp. 884–897, Mar 2013.
- [15] R. Hartley and A. Zisserman, *Multiple View Geometry in Computer Vision*, 2nd ed. Cambridge University Press, 2004.
- [16] J.-F. Cai, H. Ji, C. Liu, and Z. Shen, “Blind motion deblurring from a single image using sparse approximation,” in *Proceedings of IEEE Conference on Computer Vision and Pattern Recognition (CVPR)*, Jun 2009, pp. 104–111.
- [17] J. F. Cai, H. Ji, C. Liu, and Z. Shen, “Framelet-based blind motion deblurring from a single image,” *IEEE Transactions on Image Processing (TIP)*, vol. 21, no. 2, pp. 562–572, Feb 2012.
- [18] S. Dai and Y. Wu, “Motion from blur,” in *Proceedings of IEEE Conference on Computer Vision and Pattern Recognition (CVPR)*, Jun 2008, pp. 1–8.
- [19] Q. Shan, W. Xiong, and J. Jia, “Rotational motion deblurring of a rigid object from a single image,” in *Proceedings of IEEE International Conference on Computer Vision (ICCV)*, Oct 2007, pp. 1–8.
- [20] J. Wright, A. Yang, A. Ganesh, S. Sastry, and Y. Ma, “Robust face recognition via sparse representation,” *IEEE Transactions on Pattern Analysis and Machine Intelligence (TPAMI)*, vol. 31, no. 2, pp. 210–227, 2009.
- [21] M. Elad and M. Aharon, “Image denoising via sparse and redundant representations over learned dictionaries,” *IEEE Transactions on Image Processing (TIP)*, vol. 15, no. 12, pp. 3736–3745, Dec 2006.
- [22] Z. Hu, J.-B. Huang, and M.-H. Yang, “Single image deblurring with adaptive dictionary learning,” in *Proceedings of IEEE International Conference on Image Processing (ICIP)*, Sep 2010, pp. 1169–1172.
- [23] X. Chen, X. He, J. Yang, and Q. Wu, “An effective document image deblurring algorithm,” in *Proceedings of IEEE Conference on Computer Vision and Pattern Recognition (CVPR)*, Jun 2011, pp. 369–376.
- [24] B. Epshtein, E. Ofek, and Y. Wexler, “Detecting text in natural scenes with stroke width transform,” in *Proceedings of IEEE Conference on Computer Vision and Pattern Recognition (CVPR)*, Jun 2010, pp. 2963–2970.
- [25] J. Mao, H. Li, W. Zhou, S. Yan, and Q. Tian, “Scale based region growing for scene text detection,” in *Proceedings of the 21st ACM international conference on Multimedia*, Oct 2013, pp. 1007–1016.
- [26] A. Goldstein and R. Fattal, “Blur-kernel estimation from spectral irregularities,” in *Proceedings of European Conference on Computer Vision (ECCV)*, Oct 2012, pp. 622–635.
- [27] G. Liu, S. Chang, and Y. Ma, “Blind image deblurring using spectral properties of convolution operators,” *IEEE Transactions on Image Processing (TIP)*, vol. 23, no. 12, pp. 5047–5056, Dec 2014.
- [28] H. Zhang, D. Wipf, and Y. Zhang, “Multi-observation blind deconvolution with an adaptive sparse prior,” *IEEE Transactions on Pattern Analysis and Machine Intelligence (TPAMI)*, vol. 36, no. 8, pp. 1628–1643, Aug 2014.
- [29] L. Yuan, J. Sun, L. Quan, and H.-Y. Shum, “Image deblurring with blurred/noisy image pairs,” *ACM Transactions on Graphics (TOG)*, vol. 26, no. 3, Jul 2007.
- [30] X. Zhu, F. Šroubek, and P. Milanfar, “Deconvolving PSFs for a better motion deblurring using multiple images,” in *Proceedings of European Conference on Computer Vision (ECCV)*, Sep 2012, pp. 636–647.
- [31] D. Yang, X. Zhou, L. Xiao, and F. Wu, “Energy cooperation in multi-user wireless-powered relay networks,” *IET Communications*, vol. 9, no. 11, pp. 1412–1420, 2015.

- [32] D. Yang, "Wireless information and power transfer: Optimal power control in one-way and two-way relay system," *Wireless Personal Communications*, vol. 84, no. 1, pp. 1–14, 2015.
- [33] A. Levin, Y. Weiss, F. Durand, and W. Freeman, "Efficient marginal likelihood optimization in blind deconvolution," in *Proceedings of IEEE Conference on Computer Vision and Pattern Recognition (CVPR)*, Jun 2011, pp. 2657–2664.
- [34] J. P. Oliveira, M. A. Figueiredo, and J. M. Bioucas-Dias, "Blind estimation of motion blur parameters for image deconvolution," in *Proceedings of Iberian Conference on Pattern Recognition and Image Analysis, Part II*, Jun 2007, pp. 604–611.
- [35] O. Whyte, J. Sivic, A. Zisserman, and J. Ponce, "Non-uniform deblurring for shaken images," *International Journal of Computer Vision (IJCV)*, vol. 98, no. 2, pp. 168–186, 2012.
- [36] A. Gupta, N. Joshi, L. Zitnick, M. Cohen, and B. Curless, "Single image deblurring using motion density functions," in *Proceedings of European Conference on Computer Vision (ECCV)*, Sep 2010.
- [37] S. Zheng, L. Xu, and J. Jia, "Forward motion deblurring," in *Proceedings of IEEE International Conference on Computer Vision (ICCV)*, Dec 2013, pp. 1465–1472.
- [38] Y. Liu, J. Wang, S. Cho, A. Finkelstein, and S. Rusinkiewicz, "A no-reference metric for evaluating the quality of motion deblurring," *ACM Transactions on Graphics (TOG)*, vol. 32, no. 6, pp. 175:1–175:12, Nov 2013.
- [39] Y. C. Eldar, "Generalized SURE for exponential families: applications to regularization," *IEEE Transactions on Signal Processing (TSP)*, vol. 57, no. 2, pp. 471–481, Feb 2009.
- [40] S. Ramani, T. Blu, and M. Unser, "Blind optimization of algorithm parameters for signal denoising by Monte-Carlo SURE," in *Proceedings of IEEE International Conference on Acoustics, Speech and Signal Processing (ICASSP)*, Mar 2008, pp. 905–908.
- [41] D. J. Field, "Relations between the statistics of natural images and the response properties of cortical cells," *Journal of the Optical Society of America A*, vol. 4, no. 12, 1987.
- [42] G. J. Burton and I. R. Moorhead, "Color and spatial structure in natural scenes," *Applied Optics*, vol. 26, no. 1, 1987.
- [43] P. Toft, *The Radon Transform: Theory and Implementation : Ph.D. Thesis*. Department of Mathematical Modelling, Section for Digital Signal Processing, Technical University of Denmark, 1996.
- [44] L. Zhong, S. Cho, D. Metaxas, S. Paris, and J. Wang, "Handling noise in single image deblurring using directional filters," in *Proceedings of IEEE International Conference on Computer Vision and Pattern Recognition (CVPR)*, Jun 2013, pp. 612 – 619.
- [45] M. Moghaddam and M. Jamzad, "Motion blur identification in noisy images using fuzzy sets," in *Proceedings of IEEE International Symposium on Signal Processing and Information Technology (ISSPIT)*, Dec 2005, pp. 862–866.
- [46] H. Lee, A. Battle, R. Raina, and A. Y. Ng, "Efficient sparse coding algorithms," in *Advances in Neural Information Processing Systems 19*. MIT Press, 2007, pp. 801–808.
- [47] W. Zuo and Z. Lin, "A generalized accelerated proximal gradient approach for total-variation-based image restoration," *IEEE Transactions on Image Processing (TIP)*, vol. 20, no. 10, pp. 2748–2759, Oct 2011.
- [48] T. Goldstein and S. Osher, "The split bregman method for L1-regularized problems," *SIAM Journal on Imaging Sciences*, vol. 2, no. 2, pp. 323–343, 2009.
- [49] O. Whyte, J. Sivic, and A. Zisserman, "Deblurring shaken and partially saturated images," in *Proceedings of IEEE International Conference on Computer Vision Workshops (ICCV Workshops)*, Nov 2011, pp. 745–752.
- [50] M. Aharon, M. Elad, and A. Bruckstein, "K-SVD: An algorithm for designing overcomplete dictionaries for sparse representation," *IEEE Transactions on Signal Processing (TSP)*, vol. 54, no. 11, pp. 4311–4322, Nov 2006.
- [51] W. Dong, G. Shi, X. Li, L. Zhang, and X. Wu, "Image reconstruction with locally adaptive sparsity and nonlocal robust regularization," *Signal Processing: Image Communication*, vol. 27, no. 10, pp. 1109 – 1122, 2012.
- [52] D. Krishnan, T. Tay, and R. Fergus, "Blind deconvolution using a normalized sparsity measure," in *Proceedings of IEEE Conference on Computer Vision and Pattern Recognition (CVPR)*, Jun 2011, pp. 233–240.

- [53] C.-C. Chang and C.-J. Lin, "LIBSVM—a library for support vector machines." [Online]. Available: <http://www.csie.ntu.edu.tw/~cjlin/libsvm/>



Qingbo Lu received the B.S. degree from the School of Information Science and Engineering from the Southeast University, Nanjing, China, in 2011. He is currently pursuing the Ph.D. degree in the University of Science and Technology of China, Hefei, China. His current research interests include image/video processing, sparse representation, image quality assessment, and computer vision.



Wengang Zhou received the B.E. degree in electronic information engineering from Wuhan University, China, in 2006, and the Ph.D. degree in electronic engineering and information science from the University of Science and Technology of China, China, in 2011. He was a Research Intern with Internet Media Group, Microsoft Research Asia from 2008 to 2009. From 2011 to 2013, he was a Post-Doctoral Researcher with Computer Science Department, University of Texas at San Antonio. He is currently an Associate Professor with the Department of Electronic Engineering and Information Science, University of Science and Technology of China. His current research interests include multimedia information retrieval. He received the Best Paper Award from ACM ICIMCS in 2012.



Lu Fang received the B.S. degree from the University of Science and Technology of China (USTC), in 2007, and the Ph.D. degree from the Hong Kong University of Science and Technology (HKUST) in 2011. She was with Northwestern University in 2010. From 2011 to 2012, she was a post-doctoral research fellow at HKUST and the Singapore University of Technology and Design. She is currently an Associate Professor at USTC.



Houqiang Li received the B.S., M.Eng., and Ph.D. degrees in electronic engineering from the University of Science and Technology of China (USTC) in 1992, 1997, and 2000, respectively. He is currently a Professor with the Department of Electronic Engineering and Information Science, USTC. His current research interests include multimedia search, image/video analysis, and video coding and communication. He has authored or co-authored over 100 papers in journals and conferences. He served as an Associate Editor of the IEEE TRANSACTIONS ON CIRCUITS AND SYSTEMS FOR VIDEO TECHNOLOGY from 2010 to 2013, and has been with the Editorial Board of the Journal of Multimedia since 2009. He has served on technical/program committees, organizing committees, and as a Program Co-Chair, a Track or Session Chair for over 10 international conferences. He was the recipient of the Best Paper Award for Visual Communications and Image Processing in 2012, the International Conference on Internet Multimedia Computing and Service in 2012, and the International Conference on Mobile and Ubiquitous Multimedia from ACM in 2011, and a Senior Author of the Best Student Paper of the 5th International Mobile Multimedia Communications Conference (MobiMedia) in 2009.